RSC Advances

PAPER

View Article Online
View Journal | View Issue

Cite this: *RSC Adv.*, 2020, **10**, 6395

Facile fabrication of porous $BiVO_4$ hollow spheres with improved visible-light photocatalytic properties†

Jun Mao,‡[a] Qian Wu,‡[a] Feifei Tao,*[ab] Wen Xu,*[c] Tianjie Hong[a] and Yali Dong[a]

Bismuth vanadate ($BiVO_4$) hollow spheres with porous structure have been successfully fabricated by a one-step wet solution method with no surfactant and template. The structure, morphologies, and composition of the as-prepared products were studied with X-ray powder diffraction (XRD), transmission electron morphology (TEM), Brunauer–Emmett–Teller (BET), X-ray photoelectron spectroscopy (XPS) and UV-vis spectroscopy. Based upon the time-dependent experimental results, $BiVO_4$ nanospheres with hollow and solid structures can be controlled effectively through the reaction time, and a reasonable formation process was suggested in this work. Moreover, the experiment of degrading methyl orange (MO) under visible-light illumination was conducted to evaluate the photocatalytic performance of the obtained $BiVO_4$ samples. The porous $BiVO_4$ hollow spheres exhibit superior visible-light photocatalytic properties for MO degradation than other photocatalysts under irradiation, and could be reused for up to five times without significant reduction in the photocatalytic activity. In addition, based on active group trapping experiments, $^{\bullet}OH$ radicals as the main active species from H_2O_2 molecules play a vital role in the photocatalytic degradation of MO, and a photocatalytic mechanism for the $BiVO_4$ system was proposed. High photocatalytic activity, universality and stability suggest that the porous $BiVO_4$ hollow spheres may have potential applications in wastewater treatment.

Received 22nd January 2020
Accepted 4th February 2020

DOI: 10.1039/d0ra00698j

rsc.li/rsc-advances

1. Introduction

The rapid growth of the economy will inevitably give rise to environmental pollution and energy shortages. The large discharge of colored wastewater from textile, paper, rubber and other industries has posed a threat to people's health. Semiconductor photocatalysis utilizes free and inexhaustible solar energy to convert these pollutants to carbonaceous products, which provides an effective avenue for environmental purification and solar energy utilization.[1,2] As a green technology, photocatalysis has been an attractive alternative approach to treat wastewater containing colorants in the last few years.[3–5] The widely used semiconductor-based photocatalysts include zinc oxide (ZnO) and titanium dioxide (TiO_2).[6,7] However, only ultraviolet or near ultraviolet fractions of sunlight can be absorbed by ZnO and TiO_2 because of their broad bandgaps (3.0–3.2 eV). So, the development of photocatalysts with enhanced solar energy utilization efficiency is urgent.[8]

Among various kinds of visible-light photocatalysts, bismuth vanadate ($BiVO_4$) with a bandgap of about 2.4 eV was recognized as a promising visible-light-driven photocatalyst to degrade colorants.[9,10] The morphology, particle size and crystal structure of the samples significantly affect the photocatalytic properties. In the past few years, $BiVO_4$ with various micro- and nanostructures, such as fibers,[9] quantum dots,[11] nanosheets,[12] olive-like structures,[13] microtubes,[14] and hollow spheres,[15] have been prepared by some controlled methods to enhance the photocatalytic activity. And some remarkable achievements have been obtained. Compared with the solid materials, the porous and hollow structures have been extensively investigated because of their widespread promising application scenarios in multiple areas, for example catalysis,[16] molecular separation,[17] photonics,[18] and gas sensors.[19] In general, the preparation of hollow structure utilizes the removable or sacrificial hard and soft templates,[20,21] which limits the crystallization, the grain size-distribution and the purity of products because of the high temperature heat treatment. Therefore, it is scientific and practical essential to develop a template-free facile synthesis approach of porous $BiVO_4$ with hollow structure.

In this paper, bismuth vanadate ($BiVO_4$) nanospheres with porous and hollow structures were prepared with a facile and

[a]*Department of Chemistry and Chemical Engineering, Shaoxing University, Shaoxing 312000, P. R. China. E-mail: feifeitao@usx.edu.cn*

[b]*Shanghai Advanced Research Institute, Chinese Academy of Sciences, Shanghai 201210, P. R. China*

[c]*School of Chemistry and Chemical Engineering, Huangshan University, Huangshan 245041, P. R. China. E-mail: xuwen1112@163.com*

† Electronic supplementary information (ESI) available: (1) SEM images of $BiVO_4$ hollow spheres; (2) XPS spectra; (3) SEM images of $BiVO_4$ solid spheres; (4) XRD patterns; (5) effect of H_2O_2 amount on photocatalytic degradation rate of MO in the presence of $BiVO_4$ hollow spheres; (6) PL spectra. See DOI: 10.1039/d0ra00698j

‡ J. Mao and Q. Wu contributed equally.

effective template-free method, which differed from other synthesis approaches of $BiVO_4$ hollow spheres[13,22,23] in the utilization of template. To reveal the impact of morphologies on the photocatalytic activity of $BiVO_4$ samples, solid spheres were also fabricated for comparison. The results indicated the as-synthesized porous $BiVO_4$ hollow spheres presented better photocatalytic activity and stability in degrading dyes under visible-light illumination.

2. Experiment section

2.1 Reagents

Deionized water and as-received analytical grade chemical reagents were used without further purification throughout the experiment. Reactive dyes, such as reactive black R-2BG and reactive orange R-2RLN, were purchased from Zhejiang Runtu Co., Ltd, China.

2.2 Preparation of $BiVO_4$ samples

Typically, NH_4VO_3 (1.0 mmol) and $Bi(NO_3)_3 \cdot 5H_2O$ (1.0 mmol) were dispersed in 1 mL concentrated nitric acid and 15 mL deionized water under vigorous stirring. After stirring for 10 min, $NaHCO_3$ (1.56 g) was slowly added into the obtained solution with constant stirring. Another 0.5 h stirring was performed before the above suspension solution was sealed in a stainless-steel autoclave (volume 25 mL) with Teflon liner. Then, the autoclave was placed in the oven at 120 °C for 2 h, and then naturally cooled to ambient air temperature. Finally, the light yellow samples obtained by centrifugation were washed repeatedly with ethanol and distilled water for five times, and dried at 60 °C for 12 h in vacuum. The $BiVO_4$ solid spheres were prepared with the similar method to that of the porous $BiVO_4$ hollow spheres but at the reaction time of 10 min.

2.3 Characterization

The morphologies of the samples were characterized by scanning electron microscopy (SEM, Sigma300) and transmission electron microscope (TEM, JEM-1011). X-ray powder diffraction (XRD) patterns were collected by an Empyrean X-ray diffract meter with Cu Kα radiation source (λ = 0.15406 nm) for revealing the crystal phase of the samples. A X-ray photoelectron spectroscopy (XPS) in a Physical Electronics PHI 1600 spectrometer with Al Kα X-ray source (E = 1486.6 eV) was used, and the XPS analysis was carried out at a pass energy of 187.85 eV, and the C 1s peak at 284.6 eV was used to calibrate all the binding energies of the composing elements. A Micromeritics TriStar 3020 instrument was used to measure N_2 adsorption–desorption isotherms. The Brunauer–Emmett–Teller (BET) surface areas and the pore size distribution of the samples were determined by the BET method and the Barrett–Joyner–Halenda (BJH) method. A spectrophotometer (UV-2550, Shimadzu, Japan) was employed to measure the UV-vis diffused reflectance spectra of the samples with $BaSO_4$ as a reference. A Fluoromax-3 spectrometer (Horiba Scientific) was employed to measure the photoluminescence (PL) emission spectrum of samples at room temperature.

For photoelectrochemical characterizations, a CHI760E electrochemical workstation (Chenhua, Shanghai, China) was utilized to perform conventional three-electrode tests. The working electrode was prepared by ultrasound dispersion of the powder sample (1 mg) in ethanol (1 mL) for 30 min. The slurry was suspended on an F-doped tin oxide (FTO) glass substrate with 0.196 cm^2 active area drop by drop. The uniform electrode film was dried by air and then transferred to oven at 300 °C for 3 h. And a platinum wire and Ag/AgCl (saturated KCl) acted as counter electrode and reference electrode, respectively. The photocurrent properties of the photocatalysts were measured in a Na_2SO_4 aqueous solution (0.5 mol L^{-1}) at 0.6 V (*vs.* Ag/AgCl). The light source was a 300 W xenon arc lamp and placed at 10 cm distance from the electrochemical cell. All light wavelengths below 420 nm were eliminated with glass filter.

2.4 Photocatalytic activity

Typically, 10 mg of photocatalysts were suspended in the dye aqueous solution (20 mg L^{-1}, 20 mL), such as methyl orange (MO), rhodamin B (RhB), methylene blue (MB), reactive black R-2BG (RB) and reactive orange R-2RLN (RO), with the pH value of about 2.0 adjusted by concentrate hydrochloride under ultrasonication for 5 min. To reach the adsorption–desorption equilibrium on catalyst particles, the suspensions were well magnetically stirred at 300 rpm for 0.5 h in the dark before irradiation. 0.05 mL of H_2O_2 solution (30 wt%) was added into the above suspension. Then a 250 W xenon arc lamp as the light source was switched on to initiate the photocatalytic reaction and a glass filter was adopted to eliminate UV wavelengths below 420 nm. The degradation experiments were conducted at room temperature with a continuous magnetic stirring. The samples were taken from the suspensions at different time intervals, and then analyzed after the photocatalyst particles were removed by centrifugation immediately. The absorption of the centrifuged aqueous solution was measured with a UV-vis spectrophotometer to monitor the MO concentration. The photodegradation ratio (η) was obtained according to the following equation (eqn (1)).

$$\eta = \frac{C_0 - C_t}{C_0} \times 100\% \quad (1)$$

where C_0 and C_t are the concentrations of MO solution at initial time and certain irradiation time (t).

2.5 Active species trapping experiments and recycle measurements

In order to detect the active species in the photocatalytic reaction, *tert*-butyl alcohol (TBA, 1 mmol L^{-1}), benzoquinone (BQ, 1 mmol L^{-1}), or disodium ethylenediaminetetraacetate dehydrate (EDTA-2Na, 1 mmol L^{-1}) were added to the photocatalytic system to make clear the function of hydroxyl radical ($^{\bullet}OH$), superoxideradiacal ($^{\bullet}O_2^-$) and hole (h^+), respectively. The tests for the stability of $BiVO_4$ photocatalysts were performed according to the photocatalytic degradation experiments of MO. The recycling experiments were performed 5 times with the same experimental procedure and conditions as above. After

every photocatalytic cycle test, the catalysts obtained by centrifugation for the test were dried with a vacuum oven.

3. Results and discussion

3.1 Morphology and structure

SEM and TEM were adopted to observe the morphologies of the as-prepared samples, and the results are shown in Fig. S1† and 1. As shown in Fig. S1,† the sphere-like nanoparticles of about 50 nm are fabricated on a large scale. The above results are further proved by TEM image in Fig. 1a that the $BiVO_4$ particles are almost spherical nanoparticles and are intertwined with each other. Interestingly, the further enlarged TEM image in Fig. 1b shows that $BiVO_4$ nanoparticles are hollow structures with the diameter and wall thickness of about 20 nm and 5 nm. The aggregates of hollow structures with small size in Fig. 1b are favorable for the entry and exit of chemical species, and the recovery and reuse of catalyst. At the same time a big specific surface area will be created in the inner space. Therefore, it is a reasonable candidate for photocatalysts.

Fig. 1c presents the XRD pattern of the as-prepared $BiVO_4$ hollow spheres. All measured diffraction peaks in the XRD spectrum can be referred to monoclinic $BiVO_4$ according to the standard data of JCPDS file number 14-0688. The strong and sharp peaks imply that the as-prepared $BiVO_4$ hollow spheres are well crystallized. The absence of peak from other phases suggests the successful preparation of pure and single phase $BiVO_4$ crystal.

In order to further confirm the chemical composition and the surface chemical status of elements, the prepared $BiVO_4$ hollow spheres were further characterized by XPS, as shown in Fig. S2.† The typical XPS survey spectrum of $BiVO_4$ hollow spheres with distinct peaks of Bi 4f, V 2p and O 1s is displayed in Fig. S1a.† The characteristic peaks of Bi $4f_{7/2}$ and Bi $4f_{5/2}$ located at 158.9 eV and 164.5 eV prove the presence of Bi^{3+} in $BiVO_4$ hollow spheres.[24] The peaks of V $2p_{3/2}$ and V $2p_{1/2}$ at 516.5 eV and 524.0 eV are ascribed to the V^{5+} species, confirming that the element V in the sample was in pentavalent state.[24] Also, the sample showed similar XPS signals of O 1s at 529.8 eV and 532.2 eV from the O^{2-} anions in $BiVO_4$ hollow spheres.[24]

The formation process of $BiVO_4$ hollow spheres was investigated with time-dependent experiments, and the evolution process was clearly presented by the TEM images of the intermediate products, as shown in Fig. 2. At the beginning, the nanoparticles with sphere-like shape were formed after reacting for 10 min in Fig. S3.† Further observation showed that the spherical nanoparticles with about 50 nm were solid structure (Fig. 2a). These nanoparticles were intertwined with each other, which leads to a large number of pores in the product. With the increasing reaction time to 30 min (Fig. 2b), the nanoparticles with similar morphology has no changes in size. At the same time close observation shows that some small pores appear inside a small amount of nanoparticles. As shown in Fig. 2c and d, this feature became more manifest with the increase of reaction time. The inner parts of spherical nanoparticles have more and larger pores. The formation of spherical nanoparticles with uniform hollow structures was finally completed 2 h after the reaction (Fig. 1a and b). The crystalline structure of the products prepared at the reaction time of 10 min, 30 min, 60 min and 90 min were determined by XRD measurements presented in Fig. S4.† As depicted in Fig. S4,† all diffractions peaks of the as-prepared samples at the different reaction time can be well assigned to monoclinic $BiVO_4$, which is in accordance to $BiVO_4$ hollow spheres (JCPDS 14-0688). Based on the further observation of Fig. S4a and b,† it is found that the position and intensity of the diffraction peaks are almost unchanged with the extension of reaction time, indicating that the crystal structure of the products can be independent of reaction time.

The formation mechanism of $BiVO_4$ hollow spheres can be deduced as follows. When $NaHCO_3$ was slowly added in the reaction system, a large amount of CO_2 gas was generated. The gas molecules would congregate at the $BiVO_4$ nuclei and limit the further growth of crystal nucleus at the early stage. With the

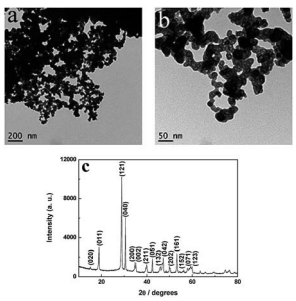

Fig. 1 TEM images (a and b) and XRD pattern (c) of the as-synthesized product.

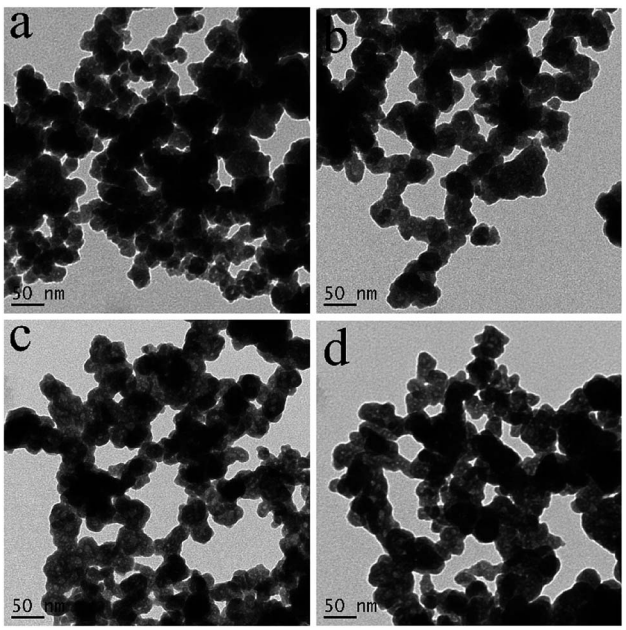

Fig. 2 TEM images of the as-prepared products at the different reaction times, (a) 10 min, (b) 30 min, (c) 60 min and (d) 90 min.

increasing reaction temperature, the expansion of gas molecules leaded to the appearance of holes in the interior of the product, which eventually forms the $BiVO_4$ hollow nanospheres. The evolution process of the morphologies of the as-synthesized products is described in Scheme 1. During the formation process of hollow structures, the internal and external pores are intertwined with one another so that $BiVO_4$ hollow spheres have a larger specific surface area, indicating the potential application in the photocatalytic field. And $BiVO_4$ hollow spheres and solid spheres can be controllably synthesized by adjusting the reaction time.

3.2 Nitrogen adsorption–desorption isotherms

The porous properties of the as-prepared $BiVO_4$ hollow spheres and solid spheres clearly revealed by the TEM images are further investigated by the nitrogen adsorption–desorption isotherms and the distribution of pore size. The $BiVO_4$ samples showed the presence of porous structure and gave type IV isotherms according to the BET classification, as shown in Fig. 3.[25] The BET specific surface area of the obtained product is 17.46 $m^2\ g^{-1}$ and 4.42 $m^2\ g^{-1}$ for $BiVO_4$ hollow spheres and $BiVO_4$ solid spheres, respectively. The increased surface area of $BiVO_4$ hollow spheres could be attributed to the porous and hollow structure. The presence of macropores and mesopores in the as-synthesized samples is indicated by the hysteresis loop in the relative pressure (p/p_0) range of 0.7 to 1 and proved by the pore size distribution (inset of Fig. 3). The calculated pore size of the $BiVO_4$ hollow spheres with BJH method ranges very widely and about at 3.8 nm, 31 nm and 117 nm, according to the adsorption branch. However, the pore size of the $BiVO_4$ solid spheres is mainly at about 70 nm. In addition, a very small number of pores are observed at about 2.5 nm. It is worth to mention here that the presence of a large number of pores will lead to a high specific surface area. A transport pathway to the interior of photocatalyst for reactants would be provided by the porous properties of the sample, and so its catalytic performance in wastewater treatment could be enhanced at the same time.

3.3 UV-vis diffuse reflection spectra

The UV-vis absorbance spectra of the obtained $BiVO_4$ samples can be found in Fig. 4. Both $BiVO_4$ hollow spheres and $BiVO_4$ solid spheres exhibit a strong photoabsorption from UV light to visible light. The steep shape of the spectra proves that the visible-light absorption was contributed to the band gap transition instead of the impurity level transition.[23] The significant visible light absorption of $BiVO_4$ hollow spheres indicates that

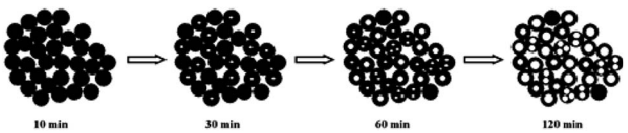

Scheme 1 Formation mechanism of the as-prepared $BiVO_4$ hollow spheres.

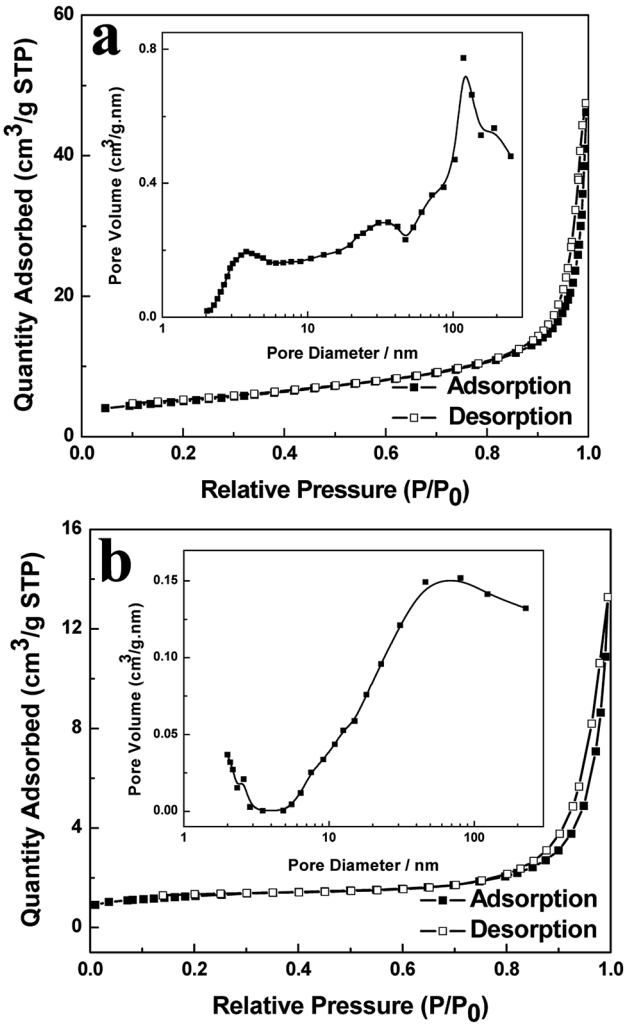

Fig. 3 Nitrogen adsorption–desorption isotherms and pore size distribution curve (inset) of $BiVO_4$ hollow spheres (a) and $BiVO_4$ solid spheres (b).

hollow structure is a better candidate than solid material in the visible-light photocatalysis. From inset of Fig. 4, the band gap energies of $BiVO_4$ hollow spheres and solid spheres could be

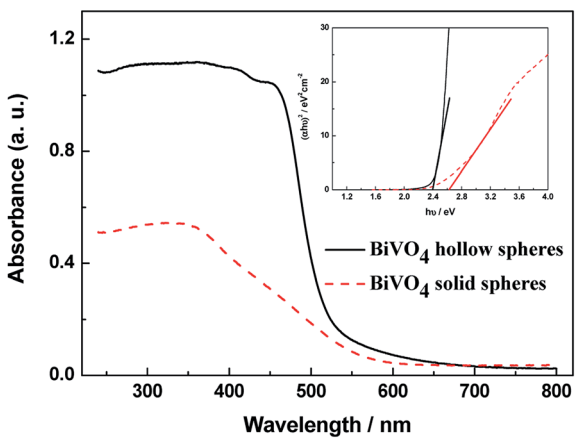

Fig. 4 UV-vis diffuse reflection spectra and plots of $(\alpha h\nu)^2$ *versus* the photon energy ($h\nu$) curves (inset) of the as-prepared $BiVO_4$ samples.

estimated from the linear fitting of the linear part of $(\alpha h\nu)2$ *vs.* $(h\nu)$ plot,[22] and are about 2.39 eV and 2.62 eV, respectively. The absorption of UV- and visible-light for exciting valence band electrons to the conduction band due to the narrow bandgap of $BiVO_4$ samples will improve the effective solar energy utilization. The band gap of $BiVO_4$ hollow spheres is narrower than that of solid ones, so the absorption and utilization of visible light energy will be stronger for $BiVO_4$ hollow spheres, thus, the higher photocatalytic activity $BiVO_4$ hollow spheres will be expected.

3.4 Photocatalytic properties

The MO degradation experiments under the visible-light irradiation were conducted to evaluate the photocatalytic activity of the as-prepared photocatalyst, as shown in Fig. 5. To demonstrate the photodegradation of MO, UV-vis spectra were taken over certain time in the presence of $BiVO_4$ hollow spheres (Fig. 5a). The photocatalytic degradation process was monitored through the intensity of characteristic absorption peak around 500 nm. With the increasing irradiation time, the characteristic peak decreases continuously in intensity and blue shifts in wavelength, indicating the decomposition of MO. And the characteristic absorption peak at about 500 nm disappears at the irritation time of 240 min, indicating the complete degradation of MO.

Fig. 5b shows the photocatalytic performance of MO in the presence of various photocatalysts. The degradation rate of 20 mg L^{-1} MO solution with 0.05 mL of H_2O_2 (30 wt%) after 4 h reaction was only about 7.27% in the absence of various photocatalyst, indicating that the photocatalyst is crucial in the photocatalytic reaction. In the presence of H_2O_2 and photocatalysts, the degradation rate of MO increases rapidly at first, then increases gently, and keeps stable finally as illumination time increased. The degradation rates of MO for as-prepared $BiVO_4$ hollow and solid spheres after 3.0 h reaction were 95.3% and 57.2%, respectively. For comparison, degrading MO experiment is conducted with the photocatalyst of P25. And about 74.2% MO was degraded under visible-light irradiation for 3 h, which is lower than $BiVO_4$ hollow spheres and slightly higher than $BiVO_4$ solid spheres. But, the degradation of MO for $BiVO_4$ hollow spheres without H_2O_2 was only 33.1% at the same irradiation conditions. The effect of H_2O_2 amount on the photocatalytic performance of MO in the presence of $BiVO_4$ hollow spheres is investigated in Fig. S5.† It can be found that with the increasing amount of H_2O_2, the photocatalytic degradation rate of MO first goes up rapidly and then tends to stabilize gradually. The further increase of H_2O_2 over 0.075 mL inhibits the photocatalytic activity, which may mainly due to the quenching of $^{\cdot}OH$ group by the excess H_2O_2.[26,27] The degradation of organic molecules with the $BiVO_4$ photocatalysts can be greatly accelerated by the radical precursor H_2O_2,[28] because H_2O_2 molecules can react with photogenerated electrons as an electron trapping reagent and the produced $^{\cdot}OH$ radicals will further react with MO and increase degradation of MO. Thus, the recombination

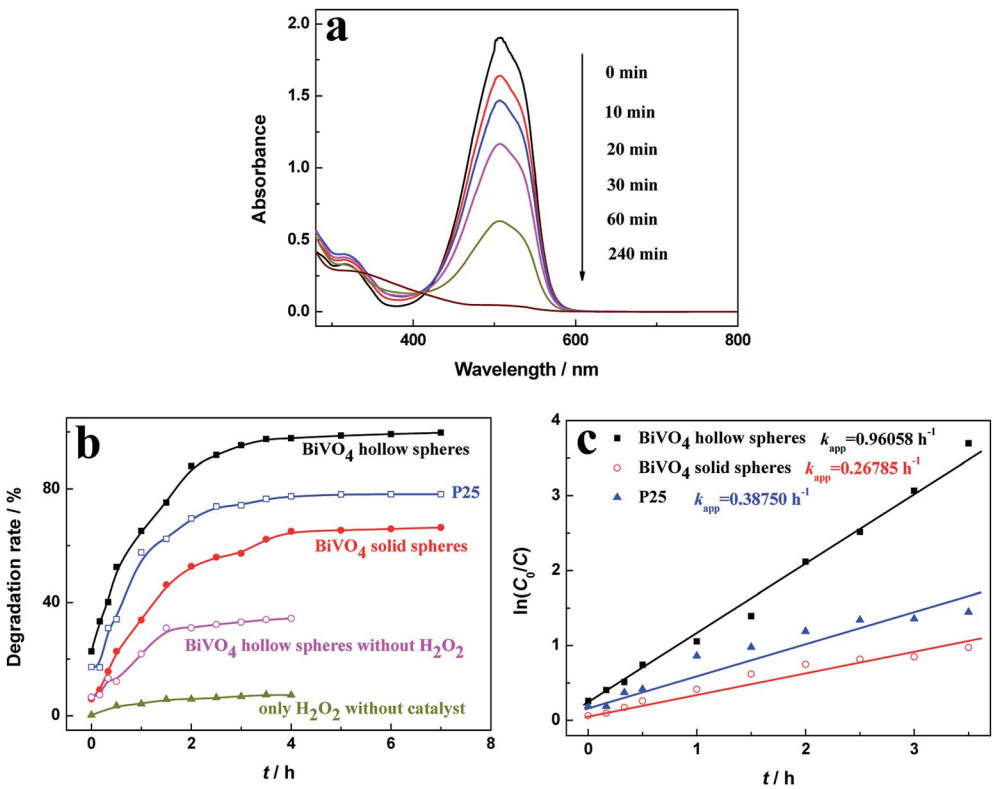

Fig. 5 (a) Absorption spectra of MO aqueous solutions in the presence of $BiVO_4$ hollow spheres, (b) degradation rate of MO at different intervals and (c) pseudo-first-order kinetic plots of MO in the presence of various photocatalysts.

of photogenerated electrons and holes will be effectively suppressed assisted by H_2O_2, leading to a high photocatalytic efficiency. In addition, the photogenerated charges must migrate to the surface of photocatalyst for the photocatalytic degradation of dyes, so large specific surface area will enhance the catalytic efficiency. Compared with $BiVO_4$ solid spheres, the significantly superior performance in the degradation of MO with $BiVO_4$ hollow spheres could be contributed to the large specific surface area due to the unique hollow and porous structures of the samples.

The pseudo first-order Langmuir–Hinshelwood (L–H) model for heterogeneous photocatalysis under low concentration dye is also used to investigate the photocatalytic degradation kinetic,[29,30] and the degradation rate (r) is given by the following equation (eqn (2)).

$$r = -\frac{dC}{dt} = K_{app}C \quad (2)$$

where K_{app} is the apparent first-order rate constant (h^{-1}), C_0 and C are the concentrations of MO at adsorption–desorption equilibrium and various intervals of time (t). Fig. 5c shows K_{app} obtained from the gradient of the curve of $\ln(C_0/C)$ *versus* time (t), and the calculated K_{app} values are 0.9606, 0.2679 and 0.3875 h^{-1} for $BiVO_4$ hollow spheres, $BiVO_4$ solid spheres and P25, respectively. The $BiVO_4$ hollow spheres exhibit the largest K_{app} value that is approximately 3.6 and 2.5 times higher than these of $BiVO_4$ solid spheres and P25, respectively. The higher photocatalytic performance of $BiVO_4$ hollow spheres over $BiVO_4$ solid spheres and P25 is agreement with that of Fig. 5b. The photocatalytic performances of $BiVO_4$ hollow spheres are further compared with other $BiVO_4$ hollow structures as summarized in Table 1. Various $BiVO_4$ samples with hollow structures can effectively degrade pollutants under their own photocatalytic reaction conditions. As compared to other $BiVO_4$ hollow catalysts, the as-prepared $BiVO_4$ hollow spheres can be highly beneficial for pollutants removal at the low concentration of photocatalyst and low light power, indicating superior performance in the visible-light photocatalysis.

In order to investigate the universality of photocatalytic performance of $BiVO_4$ samples, the photocatalytic activities of other dye aqueous solutions assisted by $BiVO_4$ hollow or solid spheres are shown in Fig. 6. At the similar experimental conditions, the degradation rates of RhB, MB, RB and RO for $BiVO_4$ hollow spheres under visible light irradiation of 4 h are more than 95%, which is obviously higher than those in the presence of $BiVO_4$ solid spheres. Based on the comparison with the $BiVO_4$ solid spheres, the $BiVO_4$ hollow spheres exhibit the outstanding photocatalytic properties for various dyes, indicating that the $BiVO_4$ nanospheres with porous and hollow structure have better universality and potential applications in visible light photocatalytic field.

To estimate the reproducibility and stability of the $BiVO_4$ samples, Fig. 7 presents the recycling test of catalyst for the visible light photocatalytic degradation of MO. The catalytic activities of $BiVO_4$ samples are almost unchanged after 5 test recycles of degradation of MO. It is found in Fig. 7 that after 5 cycles, the degradation rates of MO solution are 97.0% for $BiVO_4$ hollow spheres and 64.0% for $BiVO_4$ solid spheres, which are 99.2% and 98.5% of the first degradation rate of MO solution, respectively. This suggests that $BiVO_4$ hollow spheres have slightly better cyclic stability than $BiVO_4$ solid spheres.

3.5 Photoelectrochemical analyses

To reveal the high efficiency separation of photogenerated electrons and holes, the transient photocurrent responses of $BiVO_4$ hollow spheres and solid spheres are recorded for a few on-off illumination cycles. The higher photocurrent density implies the efficient photogenerated charge separation and their transfer across interface.[38] The I–t curves for $BiVO_4$ samples are shown in Fig. 8a for comparison. Reproducible increase under irradiation and quick recovery in the dark are observed from the photocurrent response of the $BiVO_4$ samples. Moreover, the increase of the photocurrent response of $BiVO_4$ hollow spheres is more significant in comparison with that of $BiVO_4$ solid spheres, suggesting the higher electron–hole pair separation efficiency and a smaller recombination possibility under visible-light illumination. Besides, PL spectra are used to disclose the migration, transfer, and recombination process of the photogenerated charges in the semiconductor.[22] PL spectra of $BiVO_4$ samples were recorded with a pump of 325 nm wavelength, as shown in Fig. S6.† The emission intensity of $BiVO_4$ hollow spheres with similar emission peaks is weaker than that of $BiVO_4$ solid spheres, indicating the high efficiency separation of photogenerated electron–hole pairs.

Electrochemical impedance spectroscopy (EIS) measurement has been used to reveal the efficient charge transfer process in the traditional three-electrode system[39] and corresponding Nyquist plots of $BiVO_4$ samples with and without visible light irradiation can be found in Fig. 8b. The $BiVO_4$ hollow spheres show smaller semicircle as compared to the $BiVO_4$ solid spheres with and without visible light irradiation. And it can be seen clearly that for the same sample, the radii of semicircle at illumination is smaller in size than that at darkness, implying the generation of charge carriers and low resistance as compared to dark condition. The minimum semicircle of $BiVO_4$ hollow spheres under visible light irradiation indicates the easier interfacial charge transfer between solution and electrode, and excellent conductivity, which suppresses recombination of photogenerated charge and decreases resistance. Therefore $BiVO_4$ hollow spheres could exhibit superior photocatalytic activity.

3.6 Mechanism of photocatalytic activity

Studies on active group trapping experiments give further verification of the photocatalytic activities of $BiVO_4$ hollow spheres. During the photocatalytic degradation of organic pollutants, hydroxyl radiacals ($^{\bullet}OH$), superoxide radical ($^{\bullet}O_2^-$) and hole (h^+) are generally considered as the main active species. So the reactive species trapping experiments on the photocatalytic degradation of MO are conducted to further investigate the photocatalytic mechanism over $BiVO_4$ hollow spheres. *Tert*-butyl alcohol (TBA), benzoquinone (BQ) and disodium ethylenediaminetetraacetate dehydrate (EDTA-2Na)

Table 1 Comparison of photocatalytic performances of $BiVO_4$ hollow structures

Synthesis method	Morphology	Photocatalytic activity	Ref.
Method: wet solution method Additive: no additives	Hollow nanospheres	Pollutant: MO, RhB, MB, RB, RO 10 mg photocatalyst, 20 mL 20 mg L^{-1} dye solutions Light source: 250 W Xe lamp (λ > 420 nm) Degradation: 97.8% for MO, 98.6% for RhB, 98.0% for MB, 96.5% for RB and 95.7% for RO in 4 h	This study
Method: hydrothermal route Additive: urea	Hollow microspheres	Pollutant: MB 0.1 g photocatalyst, 20 mL 3 × 10^{-5} M dye solution Light source: 350 W Xe lamp (λ > 420 nm) Degradation: color disappeared in 180 min	31
Method: a precursor solution mediated growth method Additive: polyvinyl alcohol (PVA)	Hollow spheres	Pollutant: RhB 0.5 g photocatalyst, 100 mL 10^{-4} M dye solution Light source: 120 W compact fluorescent lamp (λ > 420 nm) Degradation: characteristic peak disappears in 50 min	32
Method: solvothermal process under microwave irradiation Additive: EDTA	Hollow spheres with hierarchical microstructures	Pollutant: MO 0.2 g photocatalyst, 100 mL 0.01 g L^{-1} dye solution Light source: 300 W Xe lamp (λ > 420 nm) Degradation: characteristic absorption disappears in 180 min	33
Method: sacrificial template growth technique (calcination) Additive: carbonaceous microspheres	Multi-shell hollow spheres	Pollutant: MB 0.1 g photocatalyst, 100 mL 10^{-5} M dye solution Light source: 300 W Xe lamp (λ > 420 nm) Degradation: 100% in 80 min	34
Method: anchoring method (calcination) Additive: colloidal carbon spheres	Hollow nanospheres	Pollutant: RhB 0.1 g photocatalyst, 100 mL 10^{-5} M dye solution Light source: 500 W Xe lamp (λ > 420 nm) Degradation: completely degraded in 70 min	23
Method: hydrothermal method Additive: no additives	Core-shell structured hollow spheres	Pollutant: RhB 0.3 g photocatalyst, 600 mL 10^{-5} M dye solution Light source: 500 W Xe lamp (λ > 400 nm) Degradation: 99% in 4.5 h	35
Method: hydrothermal method Additive: ethylenediamine tetraacetic acid (EDTA)	Hollow polygon	Pollutant: MB 0.1 g photocatalyst, 100 mL 5 mg L^{-1} dye solution Light source: 500 W Xe lamp Degradation: 90.84% in 5 h	36
Method: reflux method Additive: no additives	Microtubes with flower-like morphology	Pollutant: RhB 0.5 mmol photocatalyst, 100 mL 10^{-5} M dye solution Light source: 500 W Xe lamp (λ > 400 nm) Degradation: 96% in 180 min	14
Method: ultrasound irradiation Additive: no additives	Spindle particles with hollow interior	Pollutant: RhB 0.2 g photocatalyst, 100 mL 10^{-5} M dye solution Light source: 500 W Xe lamp (λ > 400 nm) Degradation: 99% in 240 min	37

are introduced as quenchers of $^{\bullet}OH$, $^{\bullet}O_2^-$ and h^+ to make clear the effective active species in the photocatalytic process. The photocatalytic degradation rates of MO over $BiVO_4$ hollow spheres without and with the help of H_2O_2 are shown in Fig. 9. As presented in Fig. 9a, experiments involving EDTA-2Na show a significant decrease in the degradation rate in comparison to the blank experiment of no quencher, implying h^+ is the predominant active species in the absence of H_2O_2. Besides, the addition of BQ into the photocatalytic system could also decrease the photocatalytic degradation MO, suggesting $^{\bullet}O_2^-$ also plays an important role in the photocatalytic process. In order to make clear the importance of O_2 molecules, the photocatalytic reaction of MO is carried out under N_2 without any quencher. A fast deactivation of degradation rate under nitrogen suggests that O_2 molecules are involved in the photocatalytic reaction and promote the formation of $^{\bullet}O_2^-$. Therefore

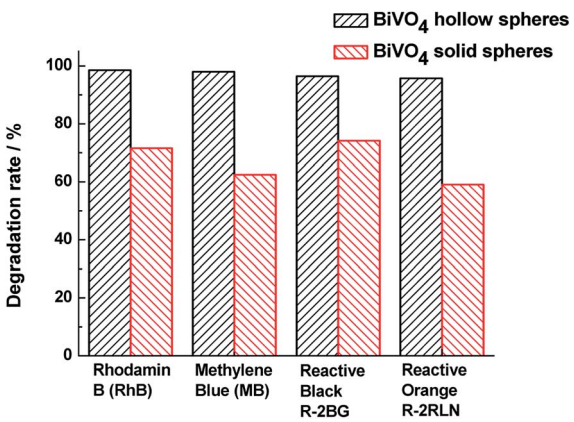

Fig. 6 Degradation rate of various dyes in the presence of $BiVO_4$ hollow or solid spheres.

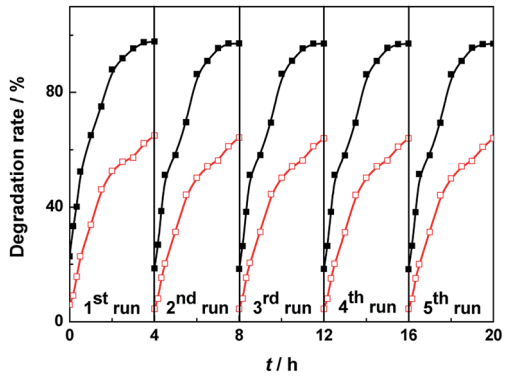

Fig. 7 Recycle curves of the $BiVO_4$ hollow spheres (black and solid) and $BiVO_4$ solid spheres (red and hollow) for the visible light photocatalytic degradation of MO.

h^+ and $^{\cdot}O_2^-$ are the mainly active groups for the photodegradation of MO without the help of H_2O_2. Compared with Fig. 9a, the photocatalytic activity of MO is significantly inhibited with TBA and decreases to 14.6% from 95.3% with the help of H_2O_2, revealing the active role played by $^{\cdot}OH$ mainly from H_2O_2. Similarly, the addition of BQ also reduces the activity and it drops to 52.4%, showing the significant impact of $^{\cdot}O_2^-$ radicals, further proved by the N_2 experiments in Fig. 9b. Based on the above analysis, the proposed photodegradation mechanism of MO over $BiVO_4$ hollow spheres is depicted in Scheme 2. $^{\cdot}OH$, $^{\cdot}O_2^-$ and h^+ are all active groups for the

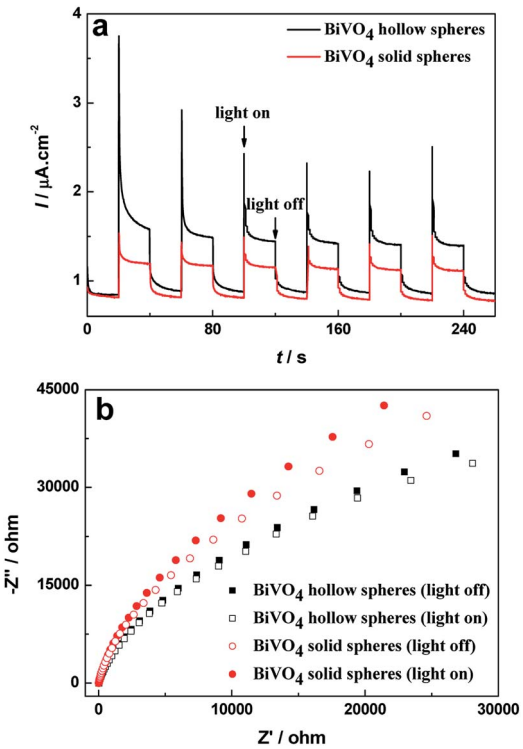

Fig. 8 (a) Transient photocurrent curves and (b) Nyquist plots of $BiVO_4$ hollow spheres and $BiVO_4$ solid spheres under dark and visible light irradiation.

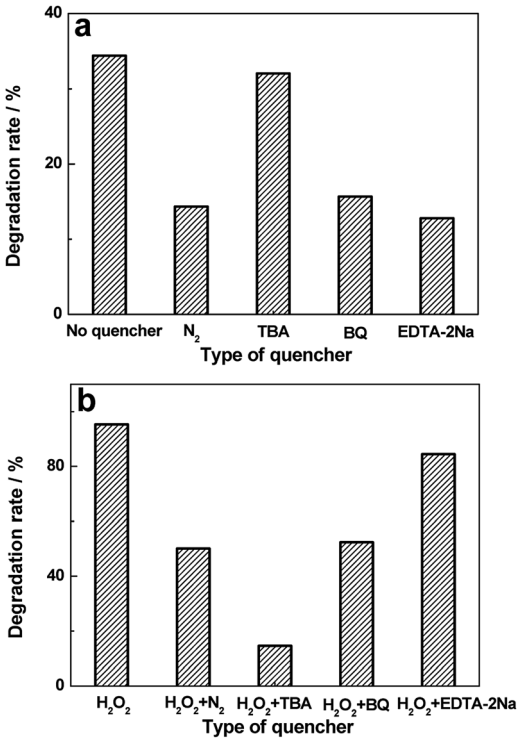

Fig. 9 Effects of a series of quenchers on the degradation rates of MO over $BiVO_4$ hollow spheres without (a) and with (b) the help of H_2O_2.

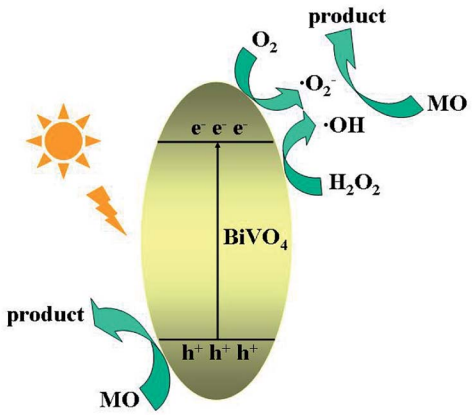

Scheme 2 The schematic diagram of the proposed photocatalytic mechanism of MO for $BiVO_4$ hollow spheres.

photocatalytic degradation of MO. Among them, $^{\cdot}OH$ radiaclas are predominantly active species with the help of H_2O_2. H_2O_2 plays an important role in the photocatalytic degradation of MO due to the presence of a large amount of $^{\cdot}OH$ radicals from H_2O_2.

4. Conclusions

Bismuth vanadate ($BiVO_4$) hollow spheres with porous structures have been fabricated by a facile template- and surfactant-free one-step wet solution method, which could be adopted to

prepare hollow structures in a large scale. Based on the time-dependent experiments, $BiVO_4$ spheres with hollow and solid structures are controlled through the reaction time and the formation process behind the synthesis of $BiVO_4$ hollow spheres is proposed. In addition, due to the distinctive morphology and narrower bandgap, $BiVO_4$ hollow spheres exhibit the outstanding visible-light photocatalytic activities and stability in the MO degradation comparing with $BiVO_4$ solid spheres. In addition, the active species trapping experiments reveal the $^{\bullet}OH$ radicals are predominantly active groups for the photocatalytic degradation of MO at the presence of H_2O_2. Overall, the obtained porous $BiVO_4$ hollow spheres with high photocatalytic activities exhibit a promising application in wastewater treatment.

Conflicts of interest

There are no conflicts to declare.

Acknowledgements

We gratefully thank the financial supports by National Natural Science Foundation of China (20901051, 51372154), Science Foundation of Ministry of Housing and Urban-Rural Development of China (2015-K4-003) and Project of Science Technology Department of Zhejiang Province of China (2017C33209).

Notes and references

1 M. Pirhashemi, S. Elhag, A. Habibi-Yangjeh, G. Pozina, M. Willander and O. Nur, Polyethylene glycol-doped $BiZn_2VO_6$ as a high-efficiency solar-light-activated photocatalyst with substantial durability toward photodegradation of organic contaminations, *RSC Adv.*, 2018, **8**(65), 37480–37491.

2 L. K. Dhandole, M. A. Mahadik, S.-G. Kim, H.-S. Chung, Y.-S. Seo, M. Cho, J. H. Ryu and J. S. Jang, Boosting photocatalytic performance of inactive rutile TiO_2 nanorods under solar light irradiation: synergistic effect of acid treatment and metal oxide co-catalysts, *ACS Appl. Mater. Interfaces*, 2017, **9**, 23602–23613.

3 Y. Cui, J. Briscoe, Y. Wang, N. V. Tarakina and S. Dunn, Enhanced photocatalytic activity of heterostructured ferroelectric $BaTiO_3$/α-Fe_2O_3 and the significance of interface morphology control, *ACS Appl. Mater. Interfaces*, 2017, **9**, 24518–24526.

4 E. Prabakaran and K. Pillay, Synthesis of N-doped ZnO nanoparticles with cabbage morphology as a catalyst for the efficient photocatalytic degradation of methylene blue under UV and visible light, *RSC Adv.*, 2019, **9**(13), 7509–7535.

5 N. Pugazhenthiran, R. V. Mangalaraja, P. Sathishkumar, S. Murugesan, T. Muneeswaran, T. Pandiyarajan, S. Naveenraj, D. Contreras and S. Anandan, Green synthesis of porous Au-N_x-TiO_2 nanospheres for solar light induced photocatalytic degradation of diazo and triazo dyes and their eco-toxic effects, *New J. Chem.*, 2018, **42**(23), 18717–18728.

6 M.-C. Wu, K.-C. Hsiao, Y.-H. Chang and K. Kordás, Core-shell heterostructures of rutile and anatase TiO_2 nanofibers for photocatalytic solar energy conversion, *ACS Appl. Nano Mater.*, 2019, **2**(4), 1970–1979.

7 J. Kegel, V. Z. Zubialevich, M. Schmidt, I. M. Povey and M. E. Pemble, Effect of surface and defect chemistry on the photocatalytic properties of intentionally defect-rich ZnO nanorod arrays, *ACS Appl. Mater. Interfaces*, 2018, **10**(21), 17994–18004.

8 H. Huang, F. Li, H. Wang and X. Zheng, The size controlled synthesis of Cu_2S/P25 hetero junction solar-energy-materials and their application in photocatalytic degradation of dyes, *RSC Adv.*, 2017, **7**(79), 50056–50063.

9 H. Liu, H. Hou, F. Gao, X. Yao and W. Yang, Tailored fabrication of thoroughly mesoporous $BiVO_4$ nanofibers and their visible-light photocatalytic activities, *ACS Appl. Mater. Interfaces*, 2016, **8**, 1929–1936.

10 T. Das, X. Rocquefelte, R. Laskowski, L. Lajaunie, S. Jobic, P. Blaha and K. Schwarz, Investigation of the optical and excitonic properties of the visible light-driven photocatalytic $BiVO_4$ material, *Chem. Mater.*, 2017, **29**, 3380–3386.

11 M. Xie, Z. Zhang, W. Han, X. Cheng, X. Li and E. Xie, Efficient hydrogen evolution under visible light irradiation over $BiVO_4$ quantum dot decorated screw-like SnO_2 nanostructures, *J. Mater. Chem. A*, 2017, **5**, 10338–10346.

12 C. Dong, S. Lu, S. Yao, R. Ge, Z. Wang, Z. Wang, P. An, Y. Liu, B. Yang and H. Zhang, Colloidal synthesis of ultrathin monoclinic $BiVO_4$ nanosheets for Z-scheme overall water splitting under visible light, *ACS Catal.*, 2018, **8**(9), 8649–8658.

13 B. Wang, L. Guo and T. He, Fabrication of an olive-like $BiVO_4$ hierarchical architecture with enhanced visible-light photocatalytic activity, *RSC Adv.*, 2016, **6**(36), 30115–30124.

14 L. Zhou, W. Wang, L. Zhang, H. Xu and W. Zhu, Single-crystalline $BiVO_4$ microtubes with square cross-sections: microstructure, growth mechanism, and photocatalytic property, *J. Phys. Chem. C*, 2007, **111**, 13659–13664.

15 J. Sun, G. Chen, J. Wu, H. Dong and G. Xiong, Bismuth vanadate hollow spheres: bubble template synthesis and enhanced photocatalytic properties for photodegradation, *Appl. Catal., B*, 2013, **132–133**, 304–314.

16 Z. Wang, Q. Wang, W. Liu, H. Ran, C. Zhang, X. Han, X. He, X. Wang and C. Hu, Optical porous hollow-boxes assembled by $SrSO_4$/TiO_2/Pt nanoparticles for high performance of photocatalytic H_2 evolution, *Nano Energy*, 2019, **59**, 129–137.

17 A. Ovcharova, V. Vasilevsky, I. Borisov, S. Bazhenov, A. Volkov, A. Bildyukevich and V. Volkov, Polysulfone porous hollow fiber membranes for ethylene-ethane separation in gas-liquid membrane contactor, *Sep. Purif. Technol.*, 2017, **183**, 162–172.

18 Y. Liu, C. Li, H. Zhang, X. Fan, Y. Liu and Q. Zhang, One-pot hydrothermal synthesis of highly monodisperse water-dispersible hollow magnetic microspheres and construction of photonic crystals, *Chem. Eng. J.*, 2015, **259**, 779–786.

19 K. Tao, X. Han, Q. Yin, D. Wang, L. Han and L. Chen, Metal–organic frameworks-derived porous In_2O_3 hollow nanorod for high-performance ethanol gas sensor, *ChemistrySelect*, 2017, **2**(33), 10918–10925.

20 X. Wang, J. Feng, Y. Bai, Q. Zhang and Y. Yin, Synthesis, properties, and applications of hollow micro-/nanostructures, *Chem. Rev.*, 2016, **116**, 10983–11060.

21 H. Zhang, H. Xu, M. Wu, Y. Zhong, D. Wang and Z. Jiao, A soft-hard template approach towards hollow mesoporous silica nanoparticles with rough surfaces for controlled drug delivery and protein adsorption, *J. Mater. Chem. B*, 2015, **3**, 6480–6489.

22 J.-Q. Li, M.-M. Cui, Z.-X. Liu, J. Du and Z.-F. Zhu, $BiVO_4$ hollow spheres with hierarchical microstructures and enhanced photocatalytic performance under visible-light illumination, *Phys. Status Solidi A*, 2013, **210**, 1881–1887.

23 W. Yin, W. Wang, M. Shang, L. Zhou, S. Sun and L. Wang, $BiVO_4$ hollow nanospheres: anchoring synthesis, growth mechanism, and their application in photocatalysis, *Eur. J. Inorg. Chem.*, 2009, (29–30), 4379–4384.

24 C. Li, P. Zhang, R. Lv, J. Lu, T. Wang, S. Wang, H. Wang and J. Gong, Selective deposition of Ag_3PO_4 on monoclinic $BiVO_4$ (040) for highly efficient photocatalysis, *Small*, 2013, **9**, 3951–3956.

25 K. S. W. Sing, D. H. Everett, R. A. W. Haul, L. Moscou, R. A. Pierotti, J. Rouquérol and T. Siemieniewska, Reporting physisorption data for gas/solid systems with special reference to the determination of surface area and porosity (Recommendations 1984), *Pure Appl. Chem.*, 1985, **57**, 603–619.

26 Y. Wang and C.-S. Hong, Effect of hydrogen peroxide, periodate and persulfate on photocatalysis of 2-chlorobiphenyl in aqueous TiO_2 suspensions, *Water Res.*, 1999, **33**, 2031–2036.

27 H. M. Coleman, V. Vimonses, G. Leslie and R. Amal, Degradation of 1,4-dioxane in water using TiO_2 based photocatalytic and H_2O_2/UV processes, *J. Hazard. Mater.*, 2007, **146**, 496–501.

28 M. Ge, L. Liu, W. Chen and Z. Zhou, Sunlight-driven degradation of rhodamine B by peanut-shaped porous $BiVO_4$ nanostructures in the H_2O_2-containing system, *CrystEngComm*, 2012, **14**, 1038–1044.

29 W. Z. Tang and H. An, UV/TiO_2 photocatalytic oxidation of commercial dyes in aqueous solutions, *Chemosphere*, 1995, **31**, 4157–4170.

30 I. M. Arabatzis, T. Stergiopoulos, D. Andreeva, S. Kitova, S. G. Neophytides and P. Falaras, Characterization and photocatalytic activity of Au/TiO_2 thin films for azo-dye degradation, *J. Catal.*, 2003, **220**, 127–135.

31 B. Cheng, W. Wang, L. Shi, J. Zhang, J. Ran and H. Yu, One-pot template-free hydrothermal synthesis of monoclinic $BiVO_4$ hollow microspheres and their enhanced visible-light photocatalytic activity, *Int. J. Photoenergy*, 2012, 797968.

32 S. Sarkar and K. K. Chattopadhyay, Visible light photocatalysis and electron emission from porous hollow spherical $BiVO_4$ nanostructures synthesized by a novel route, *Phys. E*, 2014, **58**, 52–58.

33 J.-Q. Li, M.-M. Cui, Z.-X. Liu, J. Du and Z.-F. Zhu, $BiVO_4$ hollow spheres with hierarchical microstructures and enhanced photocatalytic performance under visible-light illumination, *Phys. Status Solidi A*, 2013, **210**(9), 1881–1887.

34 L. Zong, P. Cui, F. Qin, K. Zhao, Z. Wang and R. Yu, Heterostructured bismuth vanadate multi-shell hollow spheres with high visible-light-driven photocatalytic activity, *Mater. Res. Bull.*, 2017, **86**, 44–50.

35 Y. Lu, Y.-S. Luo, H.-M. Xiao and S.-Y. Fu, Novel core-shell structured $BiVO_4$ hollow spheres with an ultra-high surface area as visible-light-driven catalyst, *CrystEngComm*, 2014, **16**(27), 6059–6065.

36 W. Ma, Z. Li and W. Liu, Hydrothermal preparation of $BiVO_4$ photocatalyst with perforated hollow morphology and its performance on methylene blue degradation, *Ceram. Int.*, 2015, **41**(3), 4340–4347.

37 W. Liu, L. Cao, G. Su, H. Liu, X. Wang and L. Zhang, Ultrasound assisted synthesis of monoclinic structured spindle $BiVO_4$ particles with hollow structure and its photocatalytic property, *Ultrason. Sonochem.*, 2010, **17**(4), 669–674.

38 Y. Liu, Y.-X. Yu and W.-D. Zhang, MoS_2/CdS heterojuction with high photoelectrochemical activity for H_2 evolution under visible light: the role of MoS_2, *J. Phys. Chem. C*, 2013, **117**(25), 12949–12957.

39 S. Kumar, A. Kumar, A. Kumar, R. Balaji and V. Krishnan, Highly efficient visible light active 2D-2D nanocomposites of N-ZnO-g-C_3N_4 for photocatalytic degradation of diverse industrial pollutants, *ChemistrySelect*, 2018, **3**(6), 1919–1932.

